A&A, 696, L14 (2025)
https://doi.org/10.1051/0004-6361/202554273
© The Authors 2025

Astronomy & Astrophysics

LETTER TO THE EDITOR

The COSMOS-Web ring: Spectroscopic confirmation of the background source at $z = 5.1$

Marko Shuntov[1,2,⋆], Shuowen Jin[1,3,⋆], Wilfried Mercier[4], Jeyhan S. Kartaltepe[5], Rebecca Larson[5], Ali Ahmad Khostovan[6,5], Raphaël Gavazzi[4,7], James W. Nightingale[8], Olivier Ilbert[4], Rafael Arango-Toro[4], Maximilien Franco[7], Hollis B. Akins[9], Caitlin M. Casey[10,9,1], Henry Joy McCracken[7], Laure Ciesla[4], Georgios E. Magdis[1,3], Aristeidis Amvrosiadis[8], Andrea Enia[11,12], Andreas L. Faisst[13], Anton M. Koekemoer[14], Clotilde Laigle[7], Damien Le Borgne[7], Richard Massey[8,15], Thibaud Moutard[4], and Mattia Vaccari[16,17,18]

(Affiliations can be found after the references)

Received 26 February 2025 / Accepted 26 March 2025

ABSTRACT

We report the spectroscopic confirmation of the background source of the most distant Einstein ring known to date, the COSMOS-Web ring. This system consists of a complete Einstein ring at $z = 5.1$, which is lensed by a massive early-type galaxy at $z \sim 2$. The redshift $z = 5.1043 \pm 0.0004$ is unambiguously identified with our NOEMA and Keck/MOSFIRE spectroscopy; the NOEMA observations reveal the CO(4–3) and CO(5–4) lines at $>8\sigma$, and the MOSFIRE data detect [O II] at $\sim 6\sigma$. Using multiwavelength photometry spanning near-infrared to radio bands, we find that the lensed galaxy is a dust-obscured starburst ($M_\star \sim 1.8 \times 10^{10}\,M_\odot$, $\mathrm{SFR_{IR}} \sim 60\,M_\odot\,\mathrm{yr}^{-1}$) with a high star formation efficiency (gas depletion time $\tau_{\rm dep} < 100$ Myr), as indicated by the [C I](1–0) non-detection. The redshift confirmation re-validates that the total lens mass budget within the Einstein radius is fully accounted for by the stellar and dark matter components, without the need of modifying the initial mass function or dark matter distribution profile. This work paves the way for detailed studies and future follow-ups of this unique lensing system, which is an ideal laboratory for studying mass distribution at $z \sim 2$ and physical conditions of star formation at $z \sim 5$.

Key words. galaxies: distances and redshifts – galaxies: high-redshift

1. Introduction

Galaxy-galaxy lensing is a powerful tool for studying both the mass distribution around the foreground lens and the physical conditions of the highly magnified background source. In an extreme case of a perfect alignment, the lensing system produces an Einstein ring, a circular image of the background sources, which is ideal for spatially resolved studies of the interstellar medium (ISM) conditions of the lensed sources. Throughout the last decade, serendipitous discoveries of strong lenses have been pushed toward increasingly higher redshifts. To date, the most distant spectroscopically confirmed lenses are at $z \sim 1.6$ (Wong et al. 2014; Cañameras et al. 2017; Ciesla et al. 2020). Among these spectacular systems, strongly magnified dusty star-forming galaxies (DSFGs) have opened a window into dust-obscured and moderate star formation activities at high redshifts (Vieira et al. 2013; Rizzo et al. 2020, 2021; Berta et al. 2021; Hamed et al. 2021; Cox et al. 2023) and provided us with unprecedented deep insights into their ISM, kinematics, and dark matter properties (e.g., Cañameras et al. 2017; Yang et al. 2017; Cava et al. 2018; Ciesla et al. 2020; Rizzo et al. 2020, 2021; Smail et al. 2023; Liu et al. 2024).

Mercier et al. (2024) report the discovery of potentially the most distant lensing system from JWST imaging, the COSMOS-Web ring, in the JWST COSMOS-Web survey (GO#1727, PIs Casey and Kartaltepe; Casey et al. 2023). The system consists of a massive ($M_\star \sim 10^{11}\,M_\odot$) and quiescent ($\mathrm{sSFR} \lesssim 10^{-13}\,\mathrm{yr}^{-1}$) early-type galaxy at $z_{\rm phot} \approx 2$. Around it is a complete Einstein ring, which is formed by the deflection of light from a background source, potentially a DSFG at $z_{\rm phot} \approx 5$. The system was also discovered independently by van Dokkum et al. (2024). However, they derived a lower $z_{\rm phot} \sim 3$ photometric redshift for the background source, which implies a significantly higher total lensing mass than a higher-redshift solution would. Thus, the exact redshift configuration of this lensing system, together with stellar mass and total dark matter mass estimates, potentially has important physical implications for the initial mass function (IMF), and even the nature of dark matter (e.g., Kong et al. 2024). Therefore, it is critical to spectroscopically confirm the redshift of the background source, which we do so here: $z = 5.10$.

In this Letter we adopt a standard Λ cold dark matter cosmology with $H_0 = 70\,\mathrm{km\,s^{-1}\,Mpc^{-1}}$, $\Omega_{\rm m} = 0.3$, and $\Omega_\Lambda = 0.7$. Physical parameters were estimated assuming a Chabrier (2003) IMF. Magnitudes are expressed in the AB system (Oke 1974).

2. Observations

First, we conducted a multi-object spectrograph (MOS) spectroscopic follow-up of the COSMOS-Web Ring using Keck/MOSFIRE in the H and K bands in December 2023, as part of program N167 (PI: J. Kartaltepe). The target was observed for 2.19 h in H and 1.72 h in K, with the slit oriented by 10° relative to the north so that it passed through the "blue" parts of the ring (see Mercier et al. 2024) and the foreground lens. The objective was to observe [O II] $\lambda\lambda$3726,3729 and Mg II $\lambda\lambda$2796,2803 in the background source if it is at $z \approx 5$

⋆ Corresponding authors: marko.shuntov@nbi.ku.dk; shuji@dtu.dk

Open Access article, published by EDP Sciences, under the terms of the Creative Commons Attribution License (https://creativecommons.org/licenses/by/4.0), which permits unrestricted use, distribution, and reproduction in any medium, provided the original work is properly cited.
This article is published in open access under the Subscribe to Open model. Subscribe to A&A to support open access publication.

(Mercier et al. 2024) or [O II], [O III] $\lambda\lambda$4959,5007, and Hβ if at $z \approx 3$ (van Dokkum et al. 2024). The 2D data were reduced and the 1D spectra were extracted using two different reduction codes: (1) following the method described in Larson et al. (2022) and (2) using PypeIt (Prochaska et al. 2020a,b). These methods are meant to reduce the contamination between the foreground lens and the background ring. In particular, we extracted two 1D spectra of the background source, one for the northern part of the ring and the other for the southern part, and did not perform a stacking of the two. The two reductions yield the same results, and we adopt the results from method (1) in this Letter since it is better tailored for high-redshift targets. We detect a 5.7σ emission line at 2.27 μm in the K band (Fig. A.1) in the northern spectrum with an equivalent width of 570 ± 40 Å. The southern spectrum shows no line detections, and therefore we omitted it from the analysis. This line would correspond to [O II] at $z = 5.10$ if $z \approx 5$ (Mercier et al. 2024), while it is not expected if $z \approx 3$ (van Dokkum et al. 2024). We do not detect Mg II, which indicates a 3σ upper limit of about 1.7 erg s^{-1} Å^{-1} cm^{-2} in the northern extraction and 1.4 erg s^{-1} Å^{-1} cm^{-2} in the southern one. However, this single line is not sufficient to robustly confirm the redshift given the photo-z discrepancy and the low S/N (see a cautionary tale by Jin et al. 2024). To definitely pin down the redshift, we carried out observations with the Institut de radioastronomie millimétrique (IRAM) interferometer, the Northern Extended Millimeter Array (NOEMA).

The NOEMA observations were executed in December 2024 (ID S24CE, PIs M. Shuntov & W. Mercier) with array configuration C and an on-source integration of 5.6 h. The frequency tunings were 72.7–82.8 GHz in the lower sideband (LSB) and 90.2–98.3 GHz in the upper sideband (USB), covering the CO(4–3), [C I](1–0), and CO(5–4) lines at $z = 5.1$. No CO line at $z \sim 3$ was covered by the tunings. Data were reduced and calibrated using the GILDAS pipeline at the IRAM headquarters in Grenoble. We produced *uv* visibility tables and performed analysis in the *uv* plane, following the methods of Jin et al. (2019, 2022). The resulting synthesized beams are ∼4.7″ × 2″ in the LSB and ∼3.7″ × 1.6″ in the USB, respectively. The calibrated data reach a line sensitivity of 0.25 mJy over a 100 km/s width at 80 GHz, and a continuum sensitivity of 6.8 μJy. Two lines are detected with S/N > 8, and dust continuum is not detected. Clean line maps were produced with the GILDAS mapping procedure `clark`. The target is not spatially resolved in the NOEMA beams, so we extracted the spectra by fitting a point source model in *uv* space at the peak position of the line maps.

3. Results

3.1. Redshift confirmation

Figure 1 presents the NOEMA line detections. Two lines are detected, at ∼75.5 GHz (8.1σ) and 94.4 GHz (9.3σ), which explicitly match the frequencies of the CO(4–3) and CO(5–4) lines at $z = 5.1$. By fitting a Gaussian profile to the two lines, we obtained consistent spectroscopic redshifts of $z_{\rm CO(5-4)} = 5.1041 \pm 0.0003$ and $z_{\rm CO(4-3)} = 5.1045 \pm 0.0004$, and the two CO lines have consistent line widths (FWHM ∼ 150 km s^{-1}). We adopted a weighted average of the two CO redshifts, $z_{\rm spec} = 5.1043 \pm 0.0004$. The redshift determined from CO lines is in excellent agreement with the redshift from MOSFIRE [O II] (Fig. A.1). This therefore spectroscopically confirms that the redshift of the lensed galaxy is $z_{\rm spec} = 5.1043 \pm 0.0004$. This redshift validates the EAZY photo-z solution of $z_{\rm phot} = 5.08^{+0.06}_{-0.04}$ from Mercier et al. (2024). The LePHARE and CIGALE $z_{\rm phot} \sim 5.5$ and $z_{\rm phot} \sim 5.3$ solutions from Mercier et al. (2024) are slightly higher than the spec-z but still agree within an uncertainty of $\Delta z/(1+z) < 0.1$. Explicitly, our results disprove the solution of $z_{\rm phot} = 2.98^{+0.42}_{-0.47}$ from van Dokkum et al. (2024).

We present the line intensity and velocity dispersion in Fig. 1 (right panels). The dust continuum and [C I](1–0) line are not detected (Fig. A.2), and we give the upper limits in Table 1.

3.2. Physical properties

With the confirmed redshift, we performed spectral energy distribution (SED) fitting to derive the physical properties of the lensed galaxy. We present the best-fit SEDs in Fig. 2, where we fit the optical + near-infrared (NIR) and radio + far-infrared (FIR) at a fixed redshift, $z = 5.1$; the best-fit results are listed in Table 1. We used the optical and NIR photometry obtained from the lens modeling using the SL_FIT code (Gavazzi et al. 2008), which measures the total and intrinsic flux of the background system, as presented by Mercier et al. (2024). This includes 15 broad bands from JWST/NIRCam, HST/ACS-F814W, CFHT/MegaCam-u, Subaru/HSC, and UltraVISTA. We measured FIR and radio photometry using our super-deblending pipeline (Jin et al. 2018; Liu et al. 2018). Because the foreground lens and the background source are not resolved in FIR or radio images, we used one prior to represent the whole system and fit the images with other sources in the same field. The de-blended photometry includes MIPS 24 μm, *Herschel*, SCUBA2 850 μm, VLA, and MeerKAT observations. We obtained S/N > 3 detections from *Herschel*/SPIRE 350 μm and 500 μm, SCUBA2 850 μm (Simpson et al. 2019), and MeerKAT 1.28 GHz data (Jarvis et al. 2016; Hale et al. 2025). Given that the foreground lens is quiescent (Mercier et al. 2024) and the lensed source shows red NIRCam colors with high dust attenuation ($E(B-V) \sim 0.7$ on the two red knots), we assumed that all FIR emissions come from the background source.

We used two methods to fit the photometry: (1) we performed a panchromatic SED fitting spanning optical to radio wavelengths with `CIGALE` (Boquien et al. 2019) assuming an energy balance between the UV and FIR, and (2) we fit only the FIR + radio photometry using the `MiChi2` code (Liu et al. 2021) without including photometry shorter than 24 μm. As shown in Fig. 2, the optical and NIR data are well fitted with `CIGALE` (blue curve), which gives a SFR = 1172 ± 209 M$_\odot$ yr^{-1} (uncorrected for magnification). However, the FIR and radio fluxes are not well modeled: the 350 μm flux was over-fit, and the 850 μm and MeerKAT fluxes were under-fit. On the other hand, the `MiChi2` fits well to the FIR and radio photometry with a template assuming a typical IR-radio scaling (Magnelli et al. 2015) and a radio slope index of −0.8. This suggests that the radio emission also originates from the background source. The `MiChi2` fitting yields a best-fit SFR$_{\rm IR}$ = 671 ± 60 M$_\odot$ yr^{-1} uncorrected for magnification, while the dust mass and temperature are largely uncertain given the poor constraints on the dust SED peak and the Rayleigh-Jeans slope. We note that the high star formation rate (SFR) from the `CIGALE` fitting could be due to the assumption of energy balance that is often not the case for DSFG SEDs. Therefore, we preferentially adopted the FIR + radio results from the `MiChi2` fitting and the optical + NIR results from the `CIGALE` fitting.

After correcting for the magnification, $\mu = 11.6$ (Mercier et al. 2024), we found that the background source has a stellar mass ($M_\star$) of $\sim 1.8 \times 10^{10}$ M$_\odot$ and an obscured SFR$_{\rm IR}$ of ∼60 M$_\odot$ yr^{-1}. The SFR is ∼1.5 times above the main sequence at $z = 5$, as constrained by recent JWST data (Cole et al. 2025).

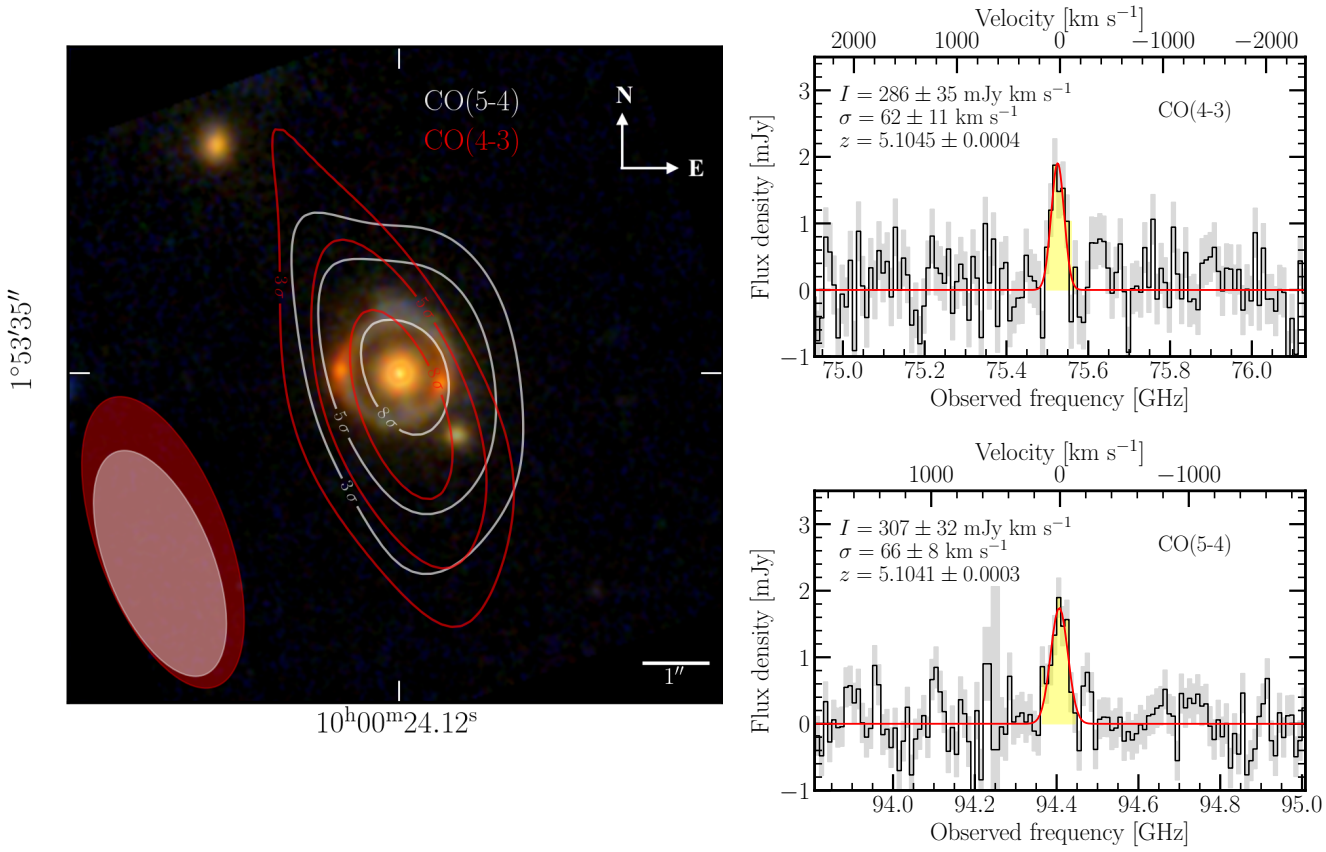

Fig. 1. Observations of the COSMOS-Web ring from HST, JWST, and NOEMA. Left: Color image composed of F444W (red), F277W (green), and a median stack of F150W + F814W (blue). Contours show the NOEMA CO maps at the 3, 5, and 8σ levels. Red and white contours correspond to CO(4–3) and CO(5–4), respectively. Ellipses in the bottom-left corner indicate the corresponding beams. Right: 1D spectra for CO(4–3) and CO(5–4) in 10 MHz/channel resolution. The flux uncertainty is shown for each channel in gray. The lines are fitted with a Gaussian profile in red; the corresponding line intensity, velocity dispersion, and redshift are presented in text.

This suggests that the galaxy could be a starburst; however, it is still within the uncertainty of the main sequence. Using [C I](1–0) as a gas tracer, we placed a 2σ upper limit of the gas mass $M_{\rm gas} < 5.1 \times 10^9\,{\rm M}_\odot$ using the [C I]-$M_{\rm gas}$ scaling from Valentino et al. (2018). With the derived ${\rm SFR_{IR}} = 58 \pm 5\,{\rm M}_\odot\,{\rm yr}^{-1}$, we obtained a gas depletion time $\tau_{\rm dep} < 100$ Myr, indicating a high star formation efficiency (SFE). This SFE is comparable to that of massive starburst galaxies at $z \sim 5$ (e.g., Ciesla et al. 2020; Riechers et al. 2020; Brinch et al. 2025), and 2–3 times higher than that of optically dark DSFGs at similar redshifts (e.g., Jin et al. 2022; Sillassen et al. 2025). This again supports its starburst nature. We note that the reconstructed source plane (Mercier et al. 2024) reveals a possible merger, in which a compact red core is likely to merge with two blue components. The high SFE is likely associated with the compact and dust-obscured component, which could be enhanced by a galaxy-galaxy merger.

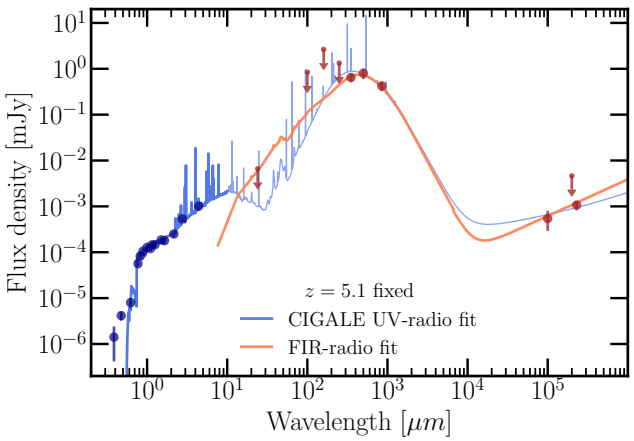

Fig. 2. SED fitting of the background source. The UV-NIR and FIR-radio fits are carried out separately by fixing $z = 5.1$. The best-fit models are shown as blue (`CIGALE`) and red (`MiChi2`) curves, respectively.

4. Discussion and conclusion

Using NOEMA and Keck/MOSFIRE spectroscopy, we have unambiguously confirmed the background source of the COSMOS-Web ring to be at $z = 5.1043 \pm 0.0004$. This is the most distant Einstein ring system known to date, in terms of both the foreground lens ($z \sim 2$) and the background source ($z = 5.1$); its detection was made possible thanks to the exquisite capability of JWST to detect distant galaxy-galaxy lenses (Nightingale et al. 2025; Mahler et al. 2025; Hogg et al. 2025). The redshift from the MOSFIRE spectrum was extracted on the blue component and is in excellent agreement with the NOEMA redshift from the CO lines that likely come from the red component. Using multiwavelength photometry spanning NIR to radio bands, we find that the background galaxy is a dust-obscured starburst

Table 1. Properties of the background source.

RA	$10^h00^m24.12^s$
Dec	$1°53'34.8''$
z_{spec}	5.1043 ± 0.0004
μ	11.6
$I_{[C\,I](1-0)}$ [mJy km s^{-1}]	<5.7
$S_{3.5\,mm}$ [μJy]	<1.2
$E(B-V)$ [mag]	0.325 ± 0.003
$\log(M_*/M_\odot)$	10.26 ± 0.15
SFR_{IR} [$M_\odot$ yr^{-1}]	58 ± 5
$M_{gas,[C\,I]}$ [10^9 $M_\odot$]	<5.1
SFE [Gyr^{-1}]	>10.2
τ_{dep} [Myr]	<96

Notes. All parameters have been corrected for magnification, μ. Upper limits are 2σ.

($M_\star \sim 1.8 \times 10^{10}\,M_\odot$, $SFR_{IR} \sim 60\,M_\odot\,yr^{-1}$) with a high SFE ($\tau_{dep} < 100$ Myr).

The redshift confirmation of the background source at $z = 5.10$ also supports the conclusion of Mercier et al. (2024), that dark matter and stellar mass fully explain the lens mass budget: lensing estimates with a $z \sim 5$ background source yield a total lens mass within the Einstein radius $M_{tot}(<\theta_{Ein}) \sim 3.8\times10^{11}\,M_\odot$, out of which $M_\star(<\theta_{Ein}) \sim 1.2 \times 10^{11}\,M_\odot$ come from stars and $M_{dm}(<\theta_{Ein}) \sim 2.6 \times 10^{11}\,M_\odot$ come from dark matter. The results are consistent with the stellar-to-halo mass scaling relation (Shuntov et al. 2022), indicating that stars and dark matter fully account for the total mass budget of the lens, without the need of modifying the IMF or the dark matter profile (as suggested by van Dokkum et al. 2024, based on a $z_{phot} \sim 3$ solution for the background source).

The upcoming JWST NIRSpec integral field unit (IFU) observations (ID 5883, PI R. Gavazzi) will confirm the lens redshift and enable a detailed dark matter substructure reconstruction of the lens. Meanwhile, the IFU data will detect rest-frame optical lines of the background source, enabling measurements of metallicity, dust attenuation, and potential active galactic nucleus signatures. Unfortunately, no ALMA observations of this unique system exist yet. Future ALMA follow-up (e.g., CO, [C II], and continuum) would be essential to spatially resolve the background source and reveal detailed dust, gas and stellar geometry, ISM conditions, and spatially resolved kinematics.

Acknowledgements. This work is based on observations carried out under projects number S24CE with the IRAM Interferometer NOEMA. IRAM is supported by INSU/CNRS (France), MPG (Germany) and IGN (Spain). We are grateful for the help received from IRAM staff during observations and data reduction. This work was supported by a NASA Keck PI Data Award, administered by the NASA Exoplanet Science Institute. Data presented herein were obtained at the W. M. Keck Observatory from telescope time allocated to the National Aeronautics and Space Administration through the agency's scientific partnership with the California Institute of Technology and the University of California. The Observatory was made possible by the generous financial support of the W. M. Keck Foundation. The authors wish to recognize and acknowledge the very significant cultural role and reverence that the summit of Maunakea has always had within the Native Hawaiian community. We are most fortunate to have the opportunity to conduct observations from this mountain. The Cosmic Dawn Center (DAWN) is funded by the Danish National Research Foundation (DNRF140). SJ acknowledges the support from the European Union's Horizon Europe research and innovation program under the Marie Skłodowska-Curie Action grant No. 101060888. SJ and GEM acknowledge the Villum Fonden research grants 37440 and 13160. JSK and AAK acknowledge support from the National Science Foundation under Grant No. 2009572 and from NASA under award No. 80NSSC22K0854. This work was made possible by utilizing the CANDIDE cluster at the Institut d'Astrophysique de Paris. The cluster was funded through grants from the PNCG, CNES, DIM-ACAV, the Euclid Consortium, and the Danish National Research Foundation Cosmic Dawn Center (DNRF140). It is maintained by Stephane Rouberol. The French COSMOS members are partly supported by the Centre National d'Etudes Spatiales (CNES). OI acknowledges the funding of the French Agence Nationale de la Recherche for the project iMAGE (grant ANR-22-CE31-0007).

References

Berta, S., Young, A. J., Cox, P., et al. 2021, A&A, 646, A122
Boquien, M., Burgarella, D., Roehlly, Y., et al. 2019, A&A, 622, A103
Brinch, M., Jin, S., Gobat, R., et al. 2025, A&A, 694, A218
Cañameras, R., Nesvadba, N. P. H., Kneissl, R., et al. 2017, A&A, 600, L3
Casey, C. M., Kartaltepe, J. S., Drakos, N. E., et al. 2023, ApJ, 954, 31
Cava, A., Schaerer, D., Richard, J., et al. 2018, Nat. Astron., 2, 76
Chabrier, G. 2003, PASP, 115, 763
Ciesla, L., Béthermin, M., Daddi, E., et al. 2020, A&A, 635, A27
Cole, J. W., Papovich, C., Finkelstein, S. L., et al. 2025, ApJ, 979, 193
Cox, P., Neri, R., Berta, S., et al. 2023, A&A, 678, A26
Gavazzi, R., Treu, T., Koopmans, L. V. E., et al. 2008, ApJ, 677, 1046
Hale, C. L., Heywood, I., Jarvis, M. J., et al. 2025, MNRAS, 536, 2187
Hamed, M., Ciesla, L., Béthermin, M., et al. 2021, A&A, 646, A127
Hogg, N. B., Nightingale, J. W., He, Q., et al. 2025, ArXiv e-prints [arXiv:2503.08785]
Jarvis, M., Taylor, R., Agudo, I., et al. 2016, MeerKAT Science: On the Pathway to the SKA, 6
Jin, S., Daddi, E., Liu, D., et al. 2018, ApJ, 864, 56
Jin, S., Daddi, E., Magdis, G. E., et al. 2019, ApJ, 887, 144
Jin, S., Daddi, E., Magdis, G. E., et al. 2022, A&A, 665, A3
Jin, S., Sillassen, N. B., Hodge, J., et al. 2024, A&A, 690, L16
Kong, D., Yang, D., & Yu, H.-B. 2024, ApJ, 965, L19
Larson, R. L., Finkelstein, S. L., Hutchison, T. A., et al. 2022, ApJ, 930, 104
Liu, D., Daddi, E., Dickinson, M., et al. 2018, ApJ, 853, 172
Liu, D., Daddi, E., Schinnerer, E., et al. 2021, ApJ, 909, 56
Liu, D., Förster Schreiber, N. M., Harrington, K. C., et al. 2024, Nat. Astron., 8, 1181
Magnelli, B., Ivison, R. J., Lutz, D., et al. 2015, A&A, 573, A45
Mahler, G., Nightingale, J. W., Hogg, N. B., et al. 2025, ArXiv e-prints [arXiv:2503.08782]
Mercier, W., Shuntov, M., Gavazzi, R., et al. 2024, A&A, 687, A61
Nightingale, J., Mahler, G., McCleary, J., et al. 2025, MNRAS, submitted [arXiv:2503.08777]
Oke, J. B. 1974, ApJS, 27, 21
Prochaska, J. X., Hennawi, J. F., Westfall, K. B., et al. 2020a, J. Open Source Softw., 5, 2308
Prochaska, J. X., Hennawi, J., Cooke, R., et al. 2020b, https://doi.org/10.5281/zenodo.3743493
Riechers, D. A., Hodge, J. A., Pavesi, R., et al. 2020, ApJ, 895, 81
Rizzo, F., Vegetti, S., Powell, D., et al. 2020, Nature, 584, 201
Rizzo, F., Vegetti, S., Fraternali, F., Stacey, H. R., & Powell, D. 2021, MNRAS, 507, 3952
Shuntov, M., McCracken, H. J., Gavazzi, R., et al. 2022, A&A, 664, A61
Sillassen, N. B., Jin, S., Magdis, G. E., et al. 2025, A&A, 693, A309
Simpson, J. M., Smail, I., Swinbank, A. M., et al. 2019, ApJ, 880, 43
Smail, I., Dudzevičiūtė, U., Gurwell, M., et al. 2023, ApJ, 958, 36
Valentino, F., Magdis, G. E., Daddi, E., et al. 2018, ApJ, 869, 27
van Dokkum, P., Brammer, G., Wang, B., Leja, J., & Conroy, C. 2024, Nat. Astron., 8, 119
Vieira, J. D., Marrone, D. P., Chapman, S. C., et al. 2013, Nature, 495, 344
Wong, K. C., Tran, K.-V. H., Suyu, S. H., et al. 2014, ApJ, 789, L31
Yang, C., Omont, A., Beelen, A., et al. 2017, A&A, 608, A144

[1] Cosmic Dawn Center (DAWN), Denmark
[2] Niels Bohr Institute, University of Copenhagen, Jagtvej 128, 2200 Copenhagen, Denmark
[3] DTU Space, Technical University of Denmark, Elektrovej 327, 2800 Kgs., Lyngby, Denmark
[4] Aix Marseille Univ, CNRS, CNES, LAM, Marseille, France
[5] Laboratory for Multiwavelength Astrophysics, School of Physics and Astronomy, Rochester Institute of Technology, 84 Lomb Memorial Drive, Rochester, NY 14623, USA

[6] Department of Physics and Astronomy, University of Kentucky, 505 Rose Street, Lexington, KY 40506, USA
[7] Institut d'Astrophysique de Paris, UMR 7095, CNRS, Sorbonne Université, 98 bis boulevard Arago, F-75014 Paris, France
[8] Institute for Computational Cosmology, Durham University, South Road, Durham DH1 3LE, UK
[9] The University of Texas at Austin, 2515 Speedway Blvd Stop, C1400 Austin, TX 78712, USA
[10] Broida Hall, Department of Physics, University of California, Santa Barbara, Santa Barbara, CA 93106, USA
[11] University of Bologna – Department of Physics and Astronomy "Augusto Righi" (DIFA), Via Gobetti 93/2, I-40129 Bologna, Italy
[12] INAF – Osservatorio di Astrofisica e Scienza dello Spazio, Via Gobetti 93/3, I-40129 Bologna, Italy
[13] Caltech/IPAC, 1200 E. California Blvd., Pasadena, CA 91125, USA
[14] Space Telescope Science Institute, 3700 San Martin Drive, Baltimore, MD 21218, USA
[15] Centre for Extragalactic Astronomy, Durham University, South Road, Durham DH1 3LE, UK
[16] Inter-University Institute for Data Intensive Astronomy, Department of Astronomy, University of Cape Town, 7701, Rondebosch Cape Town, South Africa
[17] Inter-University Institute for Data Intensive Astronomy, Department of Physics and Astronomy, University of the Western Cape, Robert Sobukwe Road, 7535, Bellville Cape Town, South Africa
[18] INAF – Istituto di Radioastronomia, Via Gobetti 101, 40129 Bologna, Italy

Appendix A: Supporting material

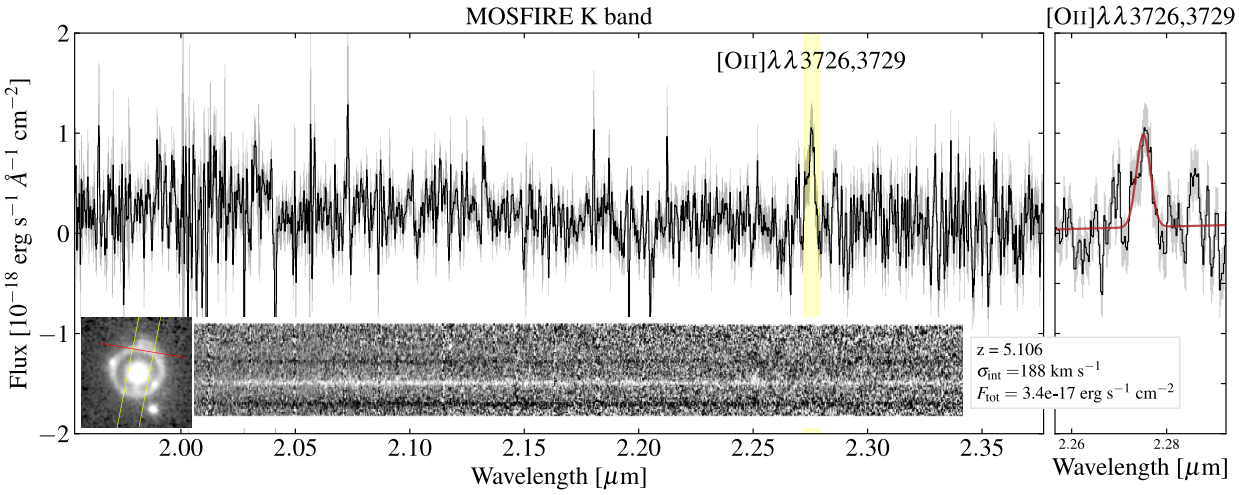

Fig. A.1. MOSFIRE spectrum of the Einstein ring. Right: Zoom-in on the [OII] doublet (S/N= 5.7) and the best-fit solution. The doublet was fitted using two Gaussian profiles separated by 3Å, with similar dispersion, and with an amplitude ratio bound between 0.35 and 1.5. The best-fit redshift, line-spread-function-corrected dispersion, and integrated [OII] flux are indicated on the bottom right. The inset shows the slit configuration (yellow box), the location where the spectrum is extracted (red line), and the 2D spectrum.

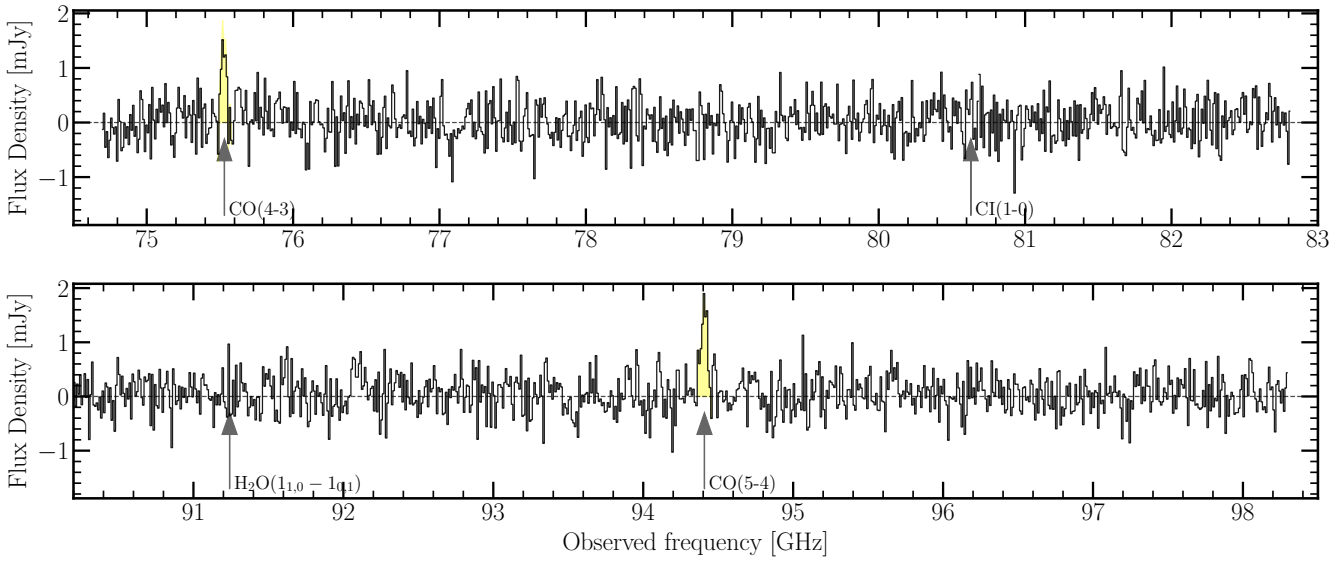

Fig. A.2. Full NOEMA spectra in the LSB (top) and USB (bottom). The arrows mark the CO and [CI] frequencies at $z = 5.1$. We highlight the CO(4-3) and CO(5-4) lines in yellow; there is no detection of [CI](1-0) or $H_2O(1_{1,0} - 1_{0,1})$.